Journal of Colloid and Interface Science 580 (2020) 785–793

Contents lists available at ScienceDirect

Journal of Colloid and Interface Science

journal homepage: www.elsevier.com/locate/jcis

Redox responsive paclitaxel dimer for programmed drug release and selectively killing cancer cells

Rui Xia [a,b], Qing Pei [a,b], Jian Wang [a,b], Zhanfeng Wang [c], Xiuli Hu [a,*], Zhigang Xie [a,b,*]

[a] State Key Laboratory of Polymer Physics and Chemistry, Changchun Institute of Applied Chemistry, Chinese Academy of Sciences, 5625 Renmin Street, Changchun, Jilin 130022, PR China
[b] University of Science and Technology of China, Hefei 230026, PR China
[c] Department of Neurosurgery, China-Japan Union Hospital of Jilin University, Changchun, Jilin 130033, PR China

HIGHLIGHTS

- Three paclitaxel dimers with alkyl sulfide, selenide or telluride are synthesized.
- Tellurium linked paclitaxel dimer exhibits superior redox responsiveness.
- Tellurium linked dimer can effectively release paclitaxel under redox stimulation.
- Tellurium linked paclitaxel dimer exhibits selective killing cancer cells ability.

GRAPHICAL ABSTRACT

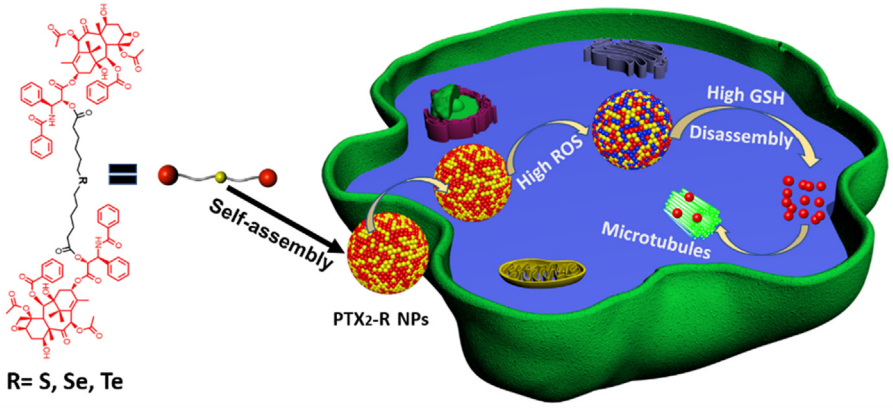

ARTICLE INFO

Article history:
Received 23 April 2020
Revised 16 July 2020
Accepted 17 July 2020
Available online 21 July 2020

Keywords:
Chemotherapy
Redox stimulus responsive
Tellurium bridged paclitaxel

ABSTRACT

Redox stimulus responsive drug delivery systems have been widely investigated and proved to be promising prospects for efficient cancer therapy due to the abnormal high level of reactive oxygen species and glutathione in tumor microenvironment. Herein, three paclitaxel dimers (named as PTX_2-R, R = S, Se and Te) bridged with alkyl sulfide, selenide or telluride are synthesized. These dimers can self-assemble into stable uniform nanoparticles (named as PTX_2-R NPs, R = S, Se and Te) with impressively high drug loading. As expected, sulfur/selenium/tellurium bonds exhibit different redox responsiveness, thereby affecting the drug release and cytotoxicity. Of note, tellurium bridged paclitaxel dimer shows ultra-sensitivity to hydrogen peroxide, which rapidly cleaves into two paclitaxel under the subsequent dithiothreitol stimulation. Our findings provide deep insight into the redox sensitivity of chalcogenide elements and offer the rational design strategies to biologically redox condition for programmed drug release.

1. Introduction

Today, cancer is still a major problem disturbing mankind [1]. People spend a lot to fight with cancer, but cancer mortality is still increasing year by year. Despite the booming researches on new cancer therapies, such as phototherapy [2] and immunotherapy

* Corresponding authors at: State Key Laboratory of Polymer Physics and Chemistry, Changchun Institute of Applied Chemistry, Chinese Academy of Sciences, 5625 Renmin Street, Changchun, Jilin 130022, PR China (Z. Xie).
E-mail addresses: lily@ciac.ac.cn (X. Hu), xiez@ciac.ac.cn (Z. Xie).

https://doi.org/10.1016/j.jcis.2020.07.086
0021-9797/

[3], traditional chemotherapies still play important role on cancer treatment [4]. However, the chemotherapies [5] are greatly limited by the drug delivery efficiency [6] and the serious side effects [7]. To solve these problems, nano drug-delivery systems (DDS) with high drug delivery efficiency have gained considerable attention [8–11]. A widely accepted concept is that ideal DDS could keep the cargoes from premature leakage during the delivery process or turn the drug into an inactive state with excellent biocompatibility. While entering the tumor area, DDS will readily release the payloads in responsive and controlled manner or effective drugs release from the prodrug stimulated by tumor microenvironment [12–17].

Compared with normal cells, tumor cells usually possess higher level of reactive oxygen species (ROS) and glutathione (GSH), leading to different redox potential, which has attracted much attention for designing tumor specific responsive DDSs [18–22]. A verity of ROS-sensitive moieties, such as thioketals, thioethers, phenylboronic acid/ester, selenium, tellurium, peroxalate ester, and GSH responsive disulfide groups have been selected and used to design tumor redox heterogeneity-triggered DDSs [23–27]. Inspired by the redox sensitivity of sulfur bonds, selenium and tellurium have also attracted increasing attention for higher sensitivity to ROS due to their lower electronegativity than sulfur [28–30]. In previous reports, several sulfur or selenium containing polymers can respond to both ROS and GSH, whereby enhance the therapeutic efficacy [31–34]. Some selenium containing polymers are able to produce ROS and induce apoptosis of cancer cells [35–36]. Tellurium containing chemical bonds have lower bond energies than selenium bond, which endows it with more sensitivity to ROS [37]. However, tellurium-based materials have been rarely investigated, especially in the field of prodrugs or dimeric drugs [38–40].

Here, three paclitaxel (PTX) dimers [41–43] bridged with sulfur, selenium, or tellurium with the same length of carbon chain are synthesized by conjugating the corresponding diacid with paclitaxel, abbreviated as PTX_2-S, PTX_2-Se, PTX_2-Te, respectively (Scheme 1). The obtained dimeric prodrugs can self-assemble into uniform nanoparticles (named as PTX_2-R NPs, R = S, Se and Te) with impressively high drug loading. The influence of sulfur/selenium/tellurium bonds on the self-assembly, stability, ROS and GSH induced drug release, cytotoxicity are compared systematically.

2. Materials and methods

2.1. Materials

Paclitaxel (>99%) was purchased from Dalian Meilun Biotechnology Co., Ltd. 1-Ethyl-3-(3-dimethylaminopropyl) carbodiimide hydrochloride (EDC·HCl) (>98%), 4-dimethylaminopyridine (DMAP) (>98%) were purchased from Energy Chemical Co., Ltd. Selenium and Tellurium (>99.9%) powders were purchased from Aladdin Co., Ltd. Sodium borohydride (>98%) were purchased from Energy Chemical Co., Ltd. 6-bromohexanoic acid (>98%) were purchased from Heowns Co., Ltd. Dithiothreitol (DTT) were purchased from Aladdin Co., Ltd. Tubulin-Tracker Red were obtained from Jiangsu KeyGEN Biotechnology Co., Ltd. Native lysis Buffer (RIPA) was purchased from Solarbio.

2.2. Characterization

Transmission electron microscope (TEM) images were carried out on a JEOL JEM–1011 (Japan) at the accelerating voltage of 100 kV. Bruker AV400 M was adopted to recorded proton nuclear magnetic resonance (^{1}H NMR) spectra at 25 °C. Malvern Zetasizer Nano was used to determine size, size distribution. Dimers detection were carried out on High performance liquid chromatography (HPLC) (SHIMADAZU, Japan). The mass spectrum (MS) analyses were performed on a LTQ ion trap mass spectrometer

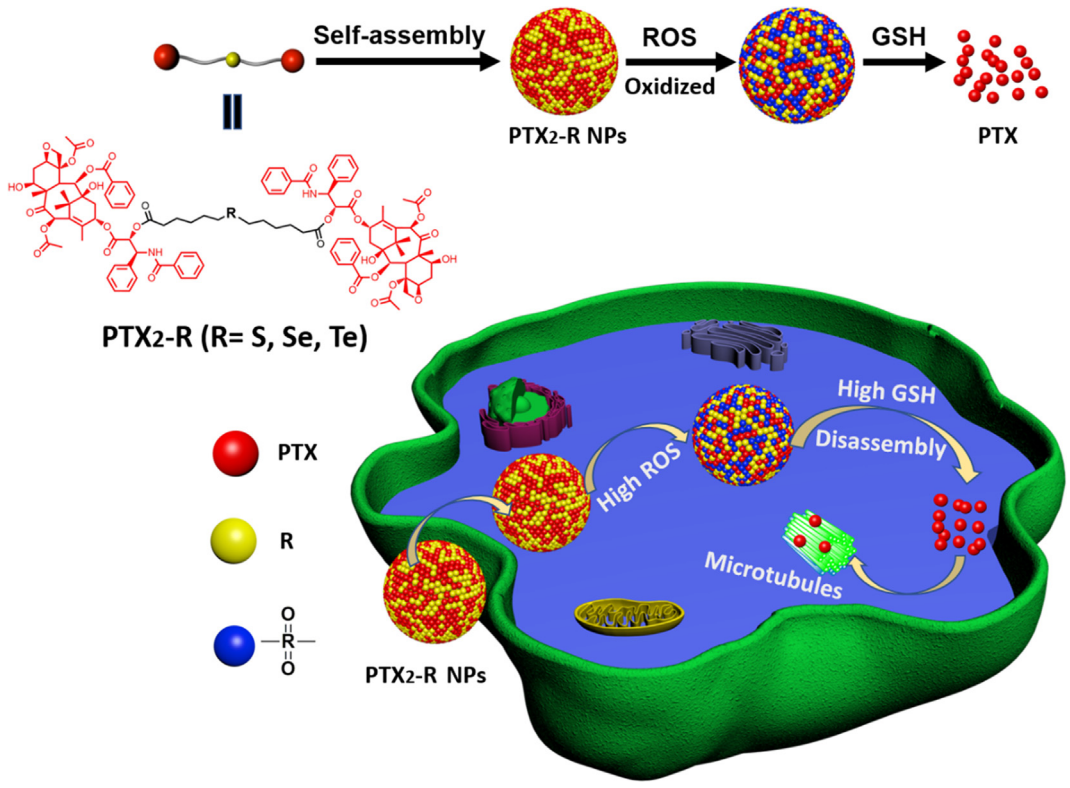

Scheme 1. Schematic illustration of the sulfur, selenium and tellurium-bridged prodrug assemblies and the proposed redox dual-responsive drug release in tumor cells.

(Finnigan, USA). Endocytosis test was carried out on confocal laser scanning microscope (CLSM) (Zeiss LSM 700, Zurich, Switzerland).

2.3. Synthesis of materials

Synthesis of $HOOCC_5$-SH and $S[(CH_2)_5COOH]_2$. 6-bromohexanoic acid (12.0 mmol, 2.34 g) and thiourea (17.7 mmol, 1.35 g) were dissolved in 30 mL ethanol. The mixture was refluxed at 85 °C under nitrogen atmosphere for 20 h. Then ethanol was evaporated and pH was adjusted to 2.0. Product was extracted with ethyl acetate and dried with magnesium sulfate. After vacuum distillation, yellowish liquid was obtained. ^{1}H NMR (400 MHz, $CDCl_3$) δ 11.76 (s, 1H), 2.48 (q, J = 7.4 Hz, 2H), 2.32 (t, J = 7.4 Hz, 2H), 1.68 – 1.52 (m, 4H), 1.46 – 1.35 (m, 2H), 1.31 (t, J = 7.8 Hz, 1H).

The yellowish liquid was dissolved in sodium hydroxide solution (7.5 M, 25 mL). 6-bromohexanoic acid (18.8 mmol, 3.66 g) was dissolved in water and dropwise added to the prepared solution at 0 °C. Then the reaction was kept at nitrogen atmosphere at 45 °C and stirred for 24 h. After that, hydrochloric acid solution was added and pH was adjusted to 1.0. The product was extracted with ethyl acetate and dried with magnesium sulfate. White solid was obtained. ^{1}H NMR (500 MHz, DMSO) δ 11.97 (s, 1H), 2.46 (t, J = 7.3 Hz, 2H), 2.23 – 2.15 (m, 2H), 1.54 – 1.45 (m, 4H), 1.37 – 1.29 (m, 2H).

Synthesis of $Se[(CH_2)_5COOH]_2$ and $Te[(CH_2)_5COOH]_2$. These two compounds were synthesized with a similar method. For the synthesis of $Te[(CH_2)_5COOH]_2$, tellurium powders (800 mg, 1 eq) were dispersed in water, sodium borohydride (600 mg, 2.5 eq) were added. The reaction was heated to 45 °C under nitrogen atmosphere. The dark solution gradually turned to pink and at last changed to a colorless transparent solution in 4 h. Then 6-bromohexanoic acid (2.7 g, 2.2 eq) in tetrahydrofuran was added and stirred overnight. After reaction, tetrahydrofuran was moved away and pH was adjusted to 4.0. Precipitation was collected and washed with water and chloroform. Light yellow powder was obtained. ^{1}H NMR (400 MHz, DMSO) δ 11.96 (s, 1H), 2.59 (t, J = 7.5 Hz, 2H), 2.19 (t, J = 7.3 Hz, 2H), 1.67 (dt, J = 14.9, 7.5 Hz, 2H), 1.51 (dt, J = 15.0, 7.3 Hz, 2H), 1.32 (dt, J = 14.8, 7.3 Hz, 2H).

$Se[(CH_2)_5COOH]_2$ was synthesized in a similar way. ^{1}H NMR (400 MHz, DMSO) δ 11.96 (s, 1H), 2.55 – 2.50 (m, 2H), 2.19 (t, J = 7.3 Hz, 2H), 1.63 – 1.53 (m, 2H), 1.49 (dd, J = 15.1, 7.5 Hz, 2H), 1.38 – 1.29 (m, 2H).

Synthesis of PTX_2-S, PTX_2-Se and PTX_2-Te dimers. These three kinds of dimers were synthesized by esterification. Specific steps were referred in our previous work [49].

For PTX_2-S, ^{1}H NMR (400 MHz, CDCl3) δ 8.18 – 8.10 (m, 2H), 7.77 – 7.70 (m, 2H), 7.61 (t, J = 7.4 Hz, 1H), 7.56 – 7.48 (m, 3H), 7.47 – 7.30 (m, 7H), 6.88 (d, J = 9.2 Hz, 1H), 6.30 (s, 1H), 6.25 (t, J = 8.9 Hz, 1H), 5.96 (d, J = 9.2, 3.2 Hz, 1H), 5.68 (d, J = 7.1 Hz, 1H), 5.51 (d, J = 3.3 Hz, 1H), 4.98 (d, J = 7.9 Hz, 1H), 4.49 – 4.41 (m, 1H), 4.32 (d, J = 8.4 Hz, 1H), 4.20 (d, J = 8.3 Hz, 1H), 3.81 (d, J = 7.0 Hz, 1H), 2.61 – 2.53 (m, 1H), 2.51 (d, J = 4.1 Hz, 1H), 2.45 (d, J = 4.2 Hz, 3H), 2.43 – 2.31 (m, 4H), 2.22 (s, 3H), 2.16 (dd, J = 15.5, 8.8 Hz, 1H), 1.98 – 1.83 (m, 4H), 1.79 (s, 1H), 1.68 (s, 3H), 1.57 – 1.47 (m, 3H), 1.36 (dd, J = 15.6, 8.7 Hz, 2H), 1.23 (s, 3H), 1.13 (s, 3H). Electrospray ionization (ESI)/MS for PTX_2-S: 1934.17 calculated, 1973.1 found, $[M + K]^+$.

For PTX_2-Se, ^{1}H NMR (500 MHz, CDCl3) δ 8.16 – 8.11 (m, 2H), 7.75 – 7.70 (m, 2H), 7.61 (t, J = 7.4 Hz, 1H), 7.50 (dt, J = 18.0, 9.2 Hz, 3H), 7.44 – 7.31 (m, 7H), 6.87 (d, J = 9.2 Hz, 1H), 6.30 (s, 1H), 6.25 (t, J = 8.6 Hz, 1H), 5.96 (dd, J = 9.2, 3.2 Hz, 1H), 5.68 (d, J = 7.1 Hz, 1H), 5.51 (d, J = 3.3 Hz, 1H), 4.97 (d, J = 8.0 Hz, 1H), 4.47 – 4.41 (m, 1H), 4.32 (d, J = 8.4 Hz, 1H), 4.20 (d, J = 8.5 Hz, 1H), 3.81 (d, J = 7.0 Hz, 1H), 2.56 (dd, J = 15.9, 9.6, 6.6 Hz, 1H), 2.52 – 2.47 (m, 2H), 2.45 (s, 4H), 2.43 – 2.32 (m, 3H), 2.22 (s, 3H), 2.19 – 2.11 (m, 1H), 1.96 – 1.84 (m, 4H), 1.72 (d, J = 5.4 Hz, 1H), 1.68 (s, 3H), 1.63 – 1.59 (m, 3H), 1.34 (dt, J = 8.2, 7.0 Hz, 2H), 1.23 (s, 3H), 1.11 (d, J = 17.6 Hz, 3H). Electrospray ionization (ESI)/MS for PTX_2-Se: 1981.07 calculated, 2015.6 found, $[M + Cl]^-$.

For PTX_2-Te, 1H NMR (500 MHz, CDCl3) δ 8.16 – 8.10 (m, 2H), 7.73 (d, J = 7.3 Hz, 2H), 7.61 (t, J = 7.4 Hz, 1H), 7.51 (dd, J = 14.9, 7.5 Hz, 3H), 7.45 – 7.31 (m, 7H), 6.89 (d, J = 9.2 Hz, 1H), 6.31 – 6.22 (m, 2H), 5.96 (dd, J = 9.2, 3.1 Hz, 1H), 5.68 (d, J = 7.1 Hz, 1H), 5.51 (d, J = 3.3 Hz, 1H), 4.97 (d, J = 8.3 Hz, 1H), 4.47 – 4.41 (m, 1H), 4.32 (d, J = 8.4 Hz, 1H), 4.20 (d, J = 8.5 Hz, 1H), 3.81 (d, J = 7.0 Hz, 1H), 2.52 (dt, J = 9.7, 6.6 Hz, 3H), 2.45 (s, 3H), 2.43 – 2.32 (m, 3H), 2.22 (d, J = 5.5 Hz, 3H), 2.19 – 2.12 (m, 1H), 1.96 – 1.85 (m, 4H), 1.80 (d, J = 4.4 Hz, 1H), 1.72 – 1.64 (m, 5H), 1.59 – 1.54 (m, 1H), 1.32 (dt, J = 15.0, 7.4 Hz, 2H), 1.21 (d, J = 15.6 Hz, 3H), 1.11 (d, J = 18.2 Hz, 3H). Electrospray ionization (ESI)/MS for PTX_2-Te: 2029.71 calculated, 2065.7 found, $[M + Cl]^-$.

2.4. Preparation of nanoparticles (NPs)

3 mg of PTX_2-S was dissolved in 3 mL of tetrahydrofuran. This solution was added dropwise into 10 mL of pure water in ten minutes, then stirred for overnight to volatilize tetrahydrofuran. At last the crude product was dialyzed against water with a 3500D dialysis bag to removal residual tetrahydrofuran. PTX_2-Se and PTX_2-Te NPs were prepared with the same method.

2.5. DTT or H_2O_2-triggered PTX release

The three kinds of dimers (60 μg) were separately dissolved in solutions (acetonitrile/water, v/v = 1/1, 500 μL) containing 10 mM DTT, 1 mM H_2O_2 or 100 μM H_2O_2 at 37 °C. At different points in time, 500 μL acetonitrile was added and solution was centrifuged at 14,000 r/min for 5 min. 20 μL supernatant was detected by HPLC to characterize the cleavage and hydrolysis of the dimers.

3. Results and discussion

3.1. Preparation and characterization of prodrug NPs

First three paclitaxel prodrug dimers were synthesized by using similar approach. Three diacid intermediates $R(C_5COOH)_2$ (R = S, Se or Te) were prepared and then conjugated with paclitaxel through esterification reaction. Scheme S1 shows the synthetic routes of sulfur/selenium/tellurium bond bridged diacid and the corresponding paclitaxel dimers. The obtained PTX_2-S, PTX_2-Se, PTX_2-Te were purified via a silica gel column with high yields (>80%) and their chemical structures were verified by nuclear magnetic resonance hydrogen spectrum (^{1}H NMR) (Figs. S1–7). The characteristic peak of 2′-hydroxyl group of PTX at 3.6 ppm disappeared, verifying the completion of esterification reaction and the reaction site was at the 2′-hydroxyl group of PTX. The particular peak values in mass spectrometry were consistent with that of theoretical calculation (Figs. S8–10), further proved the successful synthesis of these three dimers.

These obtained dimers could self-assemble into nanoparticles in aqueous solution by one-step nanoprecipitation method [44]. The three kinds of nanoparticles (PTX_2-R NPs, R = S, Se and Te) display homogeneous spherical structures, with diameters of 179.9 nm, 187.5 nm, and 204.9 nm, respectively, as measured by transmission electron microscopy (Fig. 1A, Fig. S11) and dynamic light scattering (DLS) (Fig. 1B). Detailed hydrodynamic size and polydispersity index (PDI) of PTX_2-S NPs, PTX_2-Se NPs and PTX_2-Te NPs are shown in Table S1. As the prodrugs themselves act as both the carriers and payloads, the drug loading capacity of PTX_2-R NPs is impressively high (>84 wt%). These three nanoparticles may have comparable endocytosis capacity due to their

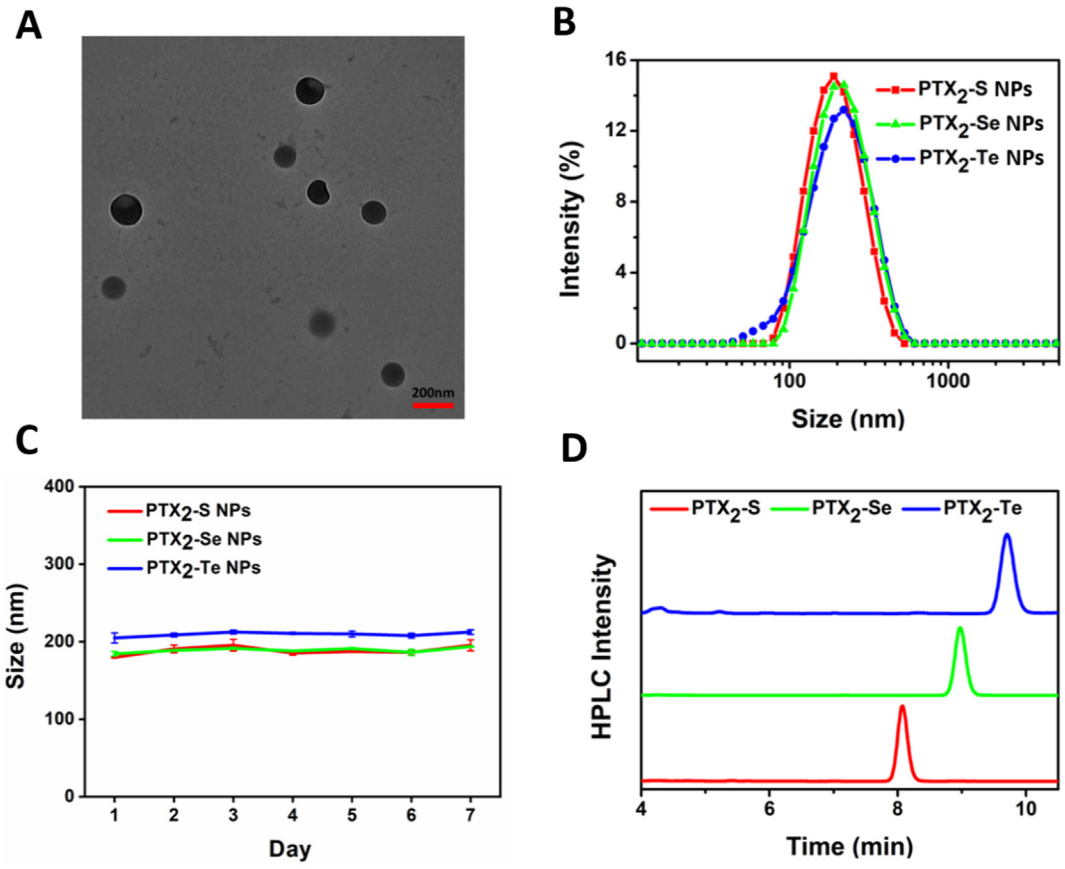

Fig. 1. (A) TEM image of PTX_2-Te NPs. (B) Size distribution of PTX_2-R NPs. (C) Size changes of PTX_2-R NPs in water for a week. (D) HPLC analysis of PTX_2-R dimers.

similar structure and particle size. The colloidal stabilities of PTX_2-R NPs were investigated and the result proves that they are stable in water for a week with a slight change of size and size distribution (Fig. 1C and Fig. S12). High performance liquid chromatography (HPLC) was used to determine the content of PTX_2-R NPs. Results display that these dimers possess various peak elution times (Fig. 1D).

3.2. DTT and GSH triggered release of PTX and speculative mechanism

As previously reported, PTX dimer bridged with thioether linker could dually respond to the tumor redox heterogeneity and gradually release PTX for chemotherapy [45–47]. We next evaluate the change of PTX_2-S, PTX_2-Se, PTX_2-Te dimers under the simulated redox environment·H_2O_2 and DTT were selected as oxidation and reduction model triggers, respectively. HPLC was employed to record the change of these dimers under redox stimulations. After incubation with 1 mM H_2O_2 for different time points, sulfur/selenium/tellurium bonds present in the dimers are gradually oxidized to form hydrophilic sulfoxide, selenoxide and tellurium oxide respectively (Fig. 2A–C). Especially for PTX_2-Te dimer, it was almost completely oxidized in an hour. Fig. S13 are the oxidation rate curves of PTX_2-S, PTX_2-Se and PTX_2-Te after incubated with 1 mM H_2O_2 for 24 h at 37 °C. We then explored the oxidation rate of three dimers incubated with 100 μM H_2O_2 which was closer to real cancer cell environment (Fig. S14). Compared with that incubated in 1 mM H_2O_2 for 24 h at 37 °C, only 10% of PTX_2-S and 50% of PTX_2-Se dimers were oxidized while PTX_2-Te is still completely oxidized in an hour. These results reveal that the oxidation rate of dimers is related to the concentration of H_2O_2 and tellurium bond is much more sensitive to H_2O_2 than sulfur and selenium bond. We guess that the largest atomic radius and weakest electronegativity endow tellurium with the lowest bond energy, leading to its superior oxidation sensitivity. This ultrasensitive character has important potential in drug delivery. In previously reported work [48], the oxidation of sulfur or selenium show excellent hydrophilicity and could facilitate the hydrolysis of the adjacent ester bond and promote drug release. However, in the present study, no apparent PTX was detected for all the three dimers even after incubation with H_2O_2 for 24 h. It's probably because the five methylene between PTX and chalcogen significantly reduce the interaction between sulfur, selenium or tellurium atoms and the ester bonds. The chalcogen in PTX dimer could only be oxidized by H_2O_2. After oxidation, the valence states of sulfur, selenium or tellurium were elevated. So the individual oxidative stimulation could not promote drug release or dimer cleavage. But this kind of chemical structures may have potential in solubility switchable materials.

Next, dithiothreitol (DTT, a prevailing simulating of GSH) was employed to monitor the degradation of dimers under reduction condition. As shown in Fig. 2D–F and Fig. S15, in the presence of 10 mM DTT, >95% of PTX_2-Te degraded in 24 h, by contast, the degradation rate of PTX_2-S and PTX_2-Se is less than 20%. Considering the extremely oxidizable nature of tellurium, we studied the interaction between PTX_2-Te and DTT in nitrogen atmosphere at 37 °C. As shown in Fig. S16, PTX_2-Te only exhibits less than 20% of degradation, meaning that PTX_2-Te alone has very weak interaction with DTT. Combining these experimental results, we propose that PTX_2-Te may be first oxidized to PTX_2-TeO or PTX_2-TeO_2 in the air at 37 °C, then the oxidation products easily react with the thiol group of DTT, leading to the degradation of PTX_2-Te (Fig. 3A). To further prove this point, we tested the mass spectra

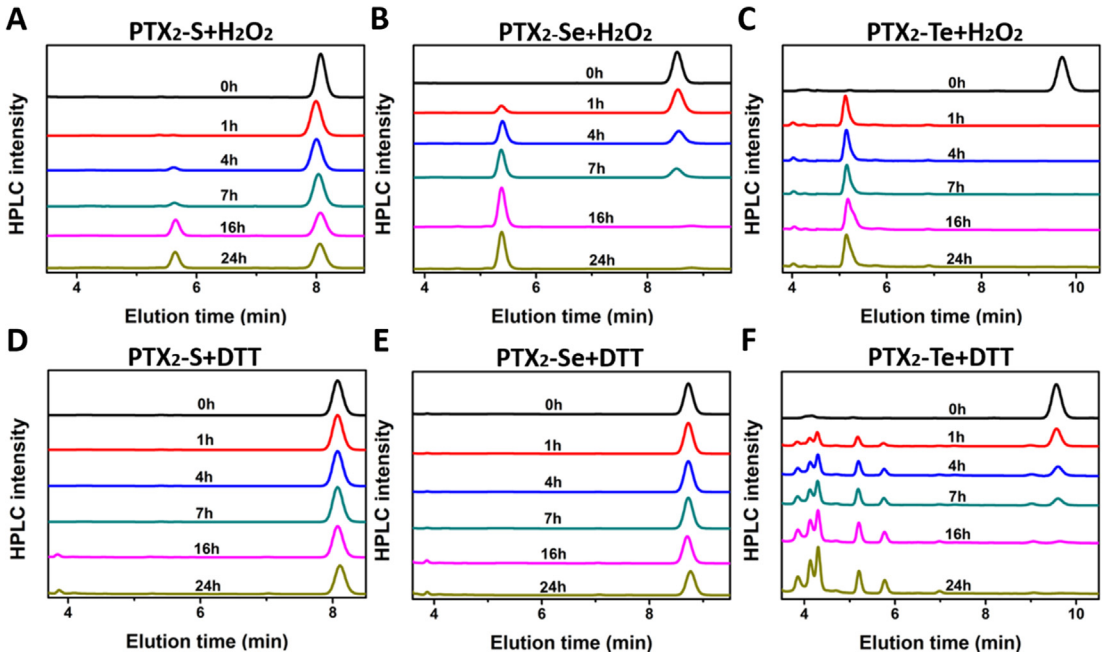

Fig. 2. HPLC analysis of PTX_2-S (A) PTX_2-Se (B) and PTX_2-Te (C) dimers in the presence of 1 mM H_2O_2 for 24 h at 37 °C. HPLC analysis of PTX_2-S (D) PTX_2-Se (E) and PTX_2-Te (F) dimers in the presence of 10 mM DTT for 24 h at 37 °C.

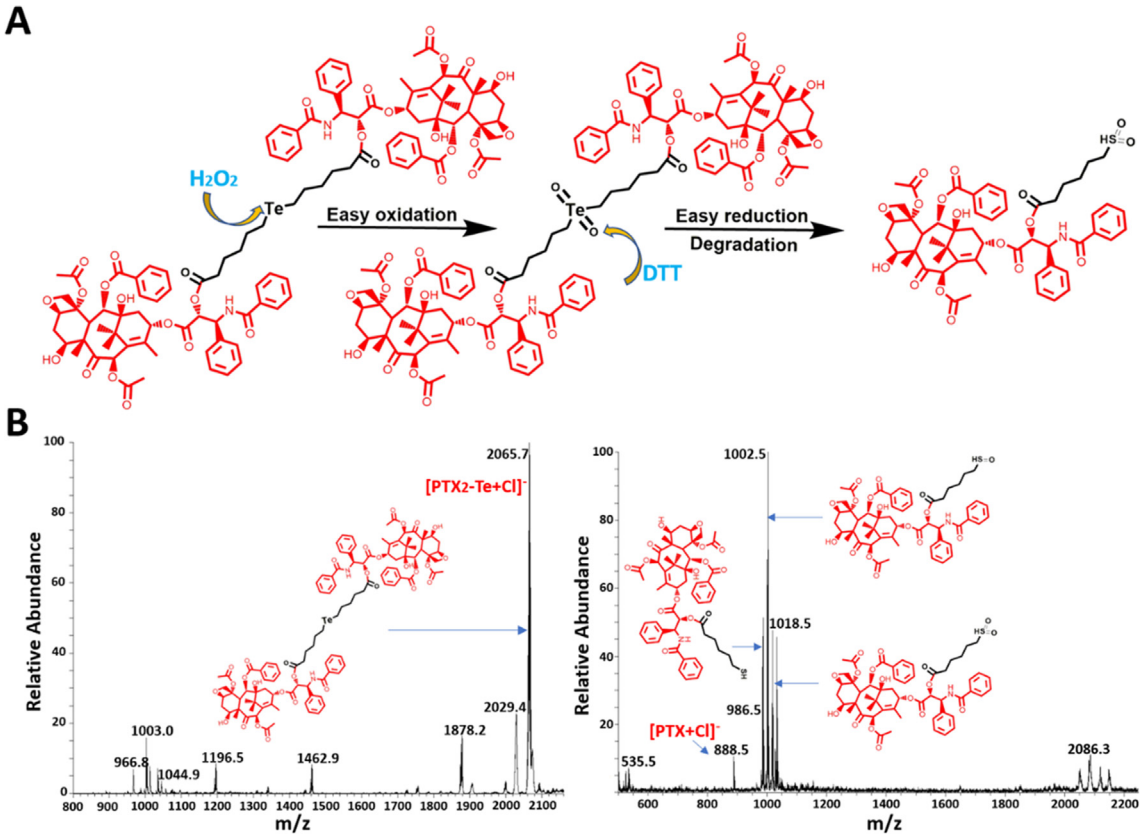

Fig. 3. (A) Proposed mechanism of the degradation of PTX_2-Te dimer stimulated by H_2O_2 and DTT. (B) Mass spectrum of PTX_2-Te with or without incubated with 10 mM DTT for 24 h at 37 °C.

of these dimers after incubation with DTT for 24 h. According to Figs. S17 and S18, no significant degradation was observed for PTX_2-S and PTX_2-Se dimers. While the characteristic peak of PTX_2-Te almost disappeared in the mass spectrum (Fig. 3B) and the molecular weight changed to 888.5 $[PTX + Na]^+$, 986.5 $[M + 2H]^{2+}$, 1002.5 $[M_{monoxide} + 2H]^{2+}$ and 1018.5 $[M_{dioxide} + 2H]^{2+}$ (M represents $PTXC_6$-SH). The result matches well with HPLC, confirming the formation of sulfoxide/sulphone and further proving

that the interaction between DTT and oxidized tellurium promotes the release of PTX. All the above results show that PTX_2-Te exhibits higher oxidation sensitivity than PTX_2-S and PTX_2-Se, and its oxidation products are more likely to be degraded under reductive stimulation. Nevertheless, PTX_2-S and PTX_2-Se are not easily oxidized in the air and the drug release ability is closely related to the distance of chalcogen atom from the ester bond. All these characteristics may make PTX_2-Te an effective redox responsive dimer, especially with methylene as little as possible.

3.3. Cellular uptake of PTX_2-R NPs

To investigate cellular uptake of PTX_2-R NPs, fluorescent dye boron dipyrromethene (BDP) was employed as a marker. Molecular structure of BDP is shown in Fig. S19. Fig. S20 shows the UV–Vis absorption and fluorescence spectra of BDP in acetone. BDP exhibits strong red fluorescence with maximum emission at 668 nm under the excitation of 555 nm laser. After co-assembly with PTX_2-S, PTX_2-Se, or PTX_2-Te dimers, BDP was encapsulated into PTX_2-R/BDP NPs. Fig. S21 shows the particle size and polydispersity index of PTX_2-R/BDP NPs. PTX_2-R/BDP NPs possess the similar sizes with PTX_2-R NPs. After incubation with HeLa cells for different time, the red fluorescence of PTX_2-R/BDP NPs was employed to monitor the endocytosis process and the blue fluorescence of 4′,6-diamidino-2-phenylindole (DAPI) was used to localize the nucleus. As shown in Fig. 4A, the internalization of PTX_2-R/BDP NPs by HeLa cells was time dependent. As time prolongs, the red fluorescence significantly enhanced. It is worth mentioning that PTX_2-R/BDP NPs showed little difference in endocytosis, which may be due to their similar structures and sizes. Fig. 4B is the statistic of their average fluorescence intensity. The effect of temperature on endocytosis was further explored. As shown in Fig. 4C**,** cells incubated with PTX_2-Te/BDP NPs at 37 °C exhibit much stronger fluorescence than that at 4 °C, indicating the endocytosis is energy-dependent.

3.4. In vitro cytotoxicity of PTX_2-R NPs

Herein, Hela cells were employed to assess the cytotoxicity of PTX_2-R NPs by using MTT assays. Because tellurium-containing compounds have been seldom investigated in cancer therapy, so we first need to investigate the biosafety of tellurium-containing diacid. As shown in Fig. 5A, Hela cells showed normal proliferative state and the cell viability was >95% even after incubation with these three diacids for 48 h. So these diacids have negligible cytotoxicity and can be well applied in nanomedicine therapy. We then tested the cytotoxicity of PTX_2-R NPs against HeLa cells. In Fig. 5B and C, PTX_2-Te NPs showed higher cytotoxicity than PTX_2-S NPs and PTX_2-Se NPs. The cell viability of PTX_2-Te NPs group is less than 16%, while it is >70% and 55% for the groups of PTX_2-S NPs and PTX_2-Se NPs, at the same concentration of 12.5 μM. All these results are consistent well with those of in vitro release experiments. In summary, due to the ultrasensitive oxidative sensitivity of PTX_2-Te, ingested into Hela cells can be easily oxidized by high intracellular ROS and further react with GSH to release PTX. But this process is difficult for insensitive PTX_2-S and PTX_2-Se, so they show unapparent cytotoxicity. It is worth mentioning that PTX_2-Te NPs showed comparable cytotoxicity to Taxol, meaning that PTX_2-Te could be cleaved into PTX to exert its cytotoxicity. Thus PTX_2-Te dimer maybe a potential effective prodrug. Furthermore, cells incubated with PTX_2-Te NPs for 48 h show obvious lower cell viability than that for 24 h. This result may be due to different endocytosis capacity of nanoparticles and the drug release process is time-dependent. Normal cells (L929 cells) were also incubated with NPs or Taxol as comparison. Similarly, the three diacids showed no significant cytotoxicity against L929 cells (Fig. 5D). Differently, PTX_2-Te NPs show significantly lower cytotoxicity against L929 cells than that against HeLa cells, at the same concentrations of PTX_2-Te NPs (Fig. 5B, C, E and F). However, Taxol maintained its significant cytotoxicity to both L929 and HeLa cells. This result may be due to the different level of redox substances in the two cell lines. Additionally, cytotoxicity of Hela cells incubated with PTX_2-R NPs under hypoxic condition was explored (Fig. S22). PTX_2-Te NPs still showed the most superior cytotoxicity among the three groups. It is worth mentioning that cytotoxicity of PTX_2-Te NPs under hypoxic condition can be comparable with that under normal oxygen condition. In detail, at the dose of 12.5 μM, the cell viability is 15.2% for normal oxygen group and 25.3% for hypoxic group. This result further proves that tellurium based prodrug may have excellent redox responsiveness to endogenous redox substances. Taking all into consideration, we believe that

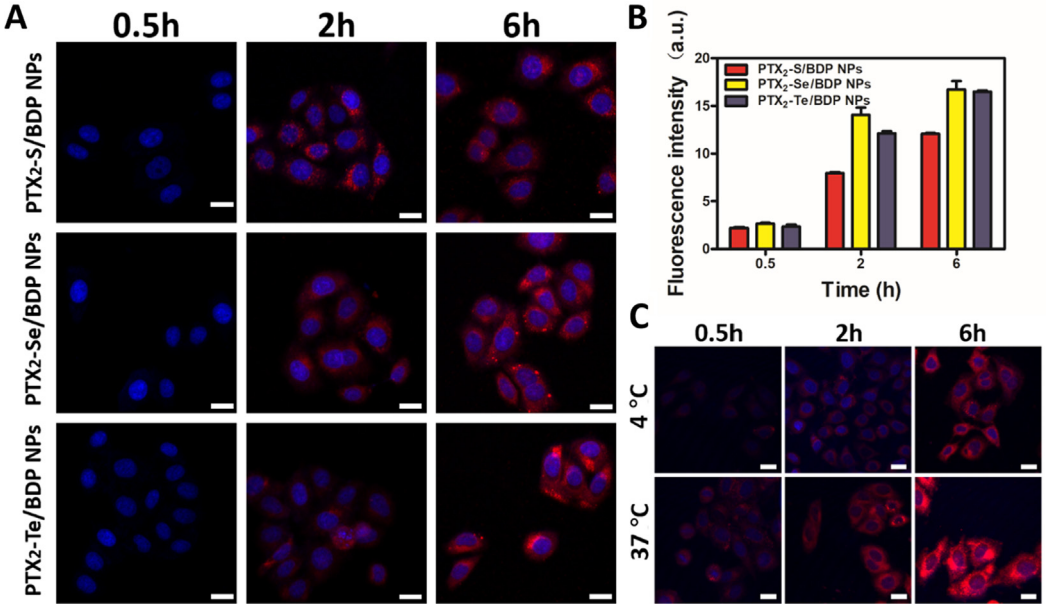

Fig. 4. Study on endocytosis of PTX_2-R/BDP NPs (n = 3). (A) Endocytosis contrast of PTX_2-R/BDP NPs at different time points. Scale bars, 20 μm. (B) Fluorescence intensity comparison of PTX_2-R/BDP NPs with different endocytosis time. (C) Comparison of endocytosis at 4 °C and 37 °C of PTX_2-Te/BDP NPs. Scale bars, 20 μm.

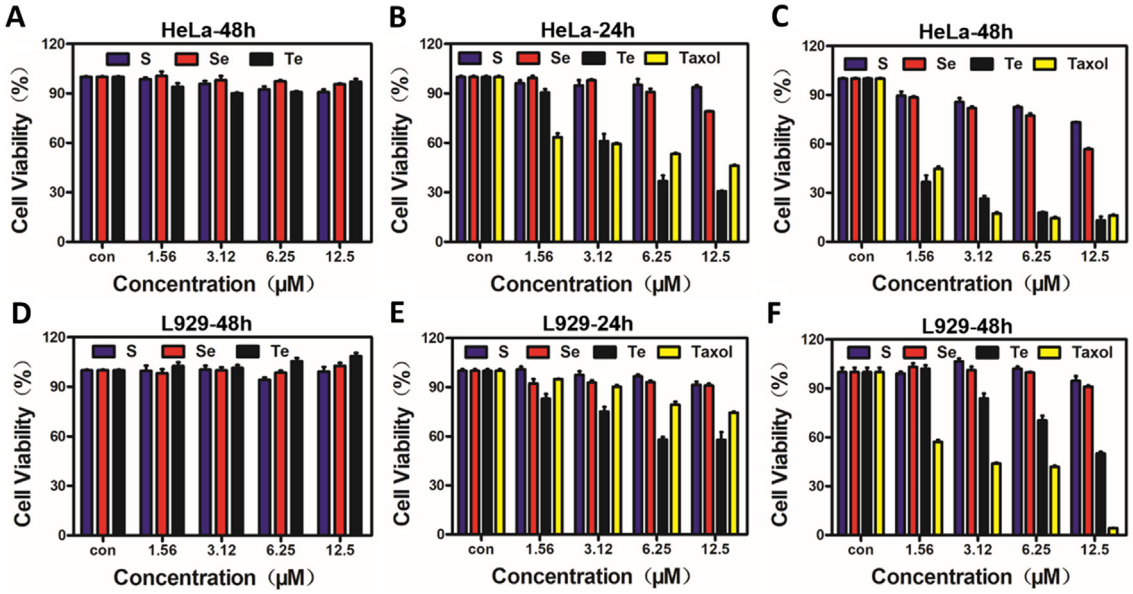

Fig. 5. In vitro cytotoxicity against HeLa cells and L929 cells (n = 4). Cytotoxicity of sulfur, selenium and tellurium based dihexanoic acid against Hela cells (A) and L929 cells (D) after incubated for 48 h. Cytotoxicity of PTX_2-S NPs, PTX_2-Se NPs and PTX_2-Te NPs against Hela cells after incubated for 24 h (B) and 48 h (C). Cytotoxicity of PTX_2-S NPs, PTX_2-Se NPs and PTX_2-Te NPs against L929 cells after incubated for 24 h (E) and 48 h (F).

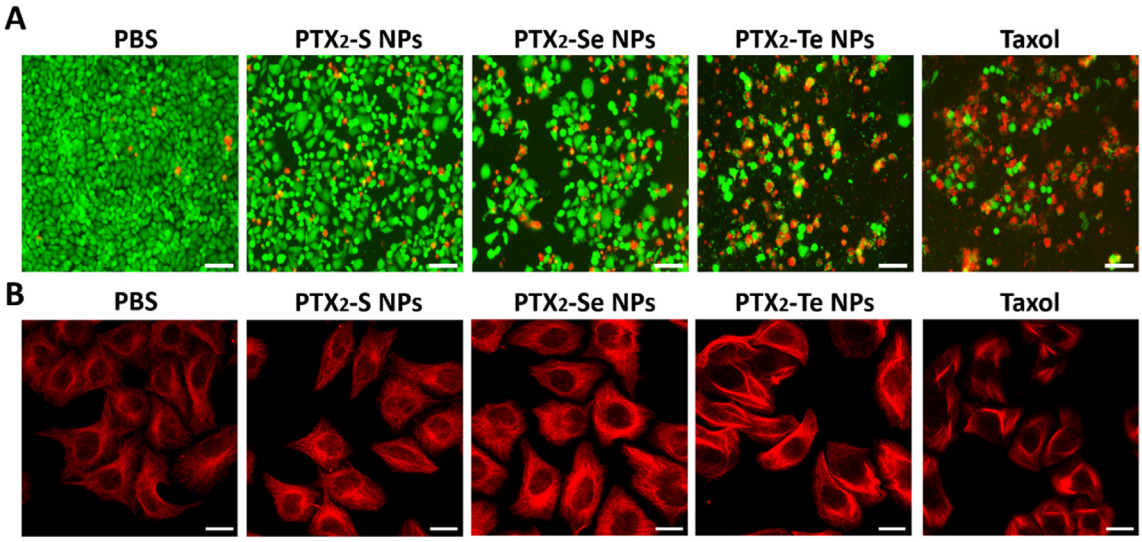

Fig. 6. Fluorescence images of Calcein-AM and propidium iodide stained HeLa cells and CLSM images of microtubule. (A) Fluorescence images of Calcein-AM and propidium iodide stained HeLa cells after treatment with three kinds of nanoparticles and Taxol for 48 h, respectively. Scale bars, 100 μm. (B) CLSM images of microtubule of HeLa cells after incubation with PBS, PTX_2-S NPs, PTX_2-Se NPs, PTX_2-Te NPs and Taxol for 12 h. Scale bars, 20 μm.

tellurium containing dimer has a faster degradation rate at the stimulation of overproduced ROS and GSH in tumor cells, leading to selective cytotoxicity against tumor cells. In normal cells, relatively low level of ROS and GSH limit the release of PTX from dimers. However, Taxol has no redox response, its high toxicity to normal cells usually would cause severe side effect. HeLa cell extracts were utilized to further investigate the degradation of prodrugs. As shown in Fig. S23, after incubated with cell extracts for 24 h, only 3% of PTX_2-Te dimers exists. As a comparison in Fig. S25, 90% of PTX_2-Te dimers still exist when incubated in phosphate buffer saline (PBS) for 24 h, meaning the rapid degradation of PTX_2-Te nanodrugs in cancer cell extracts. It is worth mentioning that the elution time of PTX_2-S and PTX_2-Se are coincided with cell extracts, so we failed to get the degradation data of PTX_2-S and PTX_2-Se nanodrugs incubated with the extract. Figs. S24 and S26 are HPLC analysis of PTX_2-S NPs, PTX_2-Se NPs and PTX_2-Te NPs incubated with cell extracts or PBS. All the cytotoxicity tests above proved that tellurium containing dimer have excellent redox responsiveness and it shows highly selective cytotoxicity against tumor cells, which may be effective to reduce the adverse side effects.

3.5. Calcein-AM/PI studies and the immunostaining assays

Cell live/death staining experiment was conducted to further verify the cytotoxicity of PTX_2-R NPs against Hela cells. Compared with the control groups, cells incubated with PTX_2-Te NPs and Taxol for 48 h showed the strongest red fluorescence from propid-

ium iodide (PI), meaning that few cells survived. And for PTX_2-Se NPs group, only a small number of cells were found dead but cell density decreased significantly. So PTX_2-Se NPs also possess a certain of cytotoxicity (Fig. 6A). Morphological transformation of microtubule induced by released PTX was tested by immunostaining assay of tubulin [49]. For the control group, the microtubule shows dispersed network structure. For Taxol and PTX_2-Te NPs groups, it changes to aggregated fascicular structure, indicating the decomposition of PTX_2-Te NPs. But for the other two groups (PTX_2-S NPs and PTX_2-Se NPs), microtubules maintained the normal reticular structure due to the difficult release of PTX (Fig. 6B). All these results proved PTX_2-Te is an effective redox responsive prodrug to release PTX and it maybe a potent antitumor prodrug in tumor treatment.

4. Conclusions

In conclusion, three PTX dimers (PTX_2-R, R = S, Se and Te) were designed and synthesized using alkyl sulfide, selenide or telluride as linkages and the corresponding nanoparticles (PTX_2-R NPs, R = S, Se and Te) were obtained. PTX_2-R NPs possess robust stability and high content of PTX, the drug content is far more than that of other nanoparticle formulations [50,51]. As we hypothesized, PTX_2-Te dimer exhibits preferable redox dual-responsive capability compared with sulfur and selenium-based paclitaxel dimers. Uniquely, tellurium-based dimer can only work under the synergetic stimulation of ROS and GSH displaying a different mechanism as reported [48]. Importantly, cell cytotoxicity test further reveals that PTX_2-Te NPs shows comparable cytotoxicity to Taxol and it displays high selective cytotoxicity against tumor cells, which is seldom seen in literature [52]. Our work gives new insight into tellurium-based redox responsive materials and may provide possibilities for the development of hypersensitive DDS for cancer therapy.

CRediT authorship contribution statement

Rui Xia: Methodology, Investigation, Software, Writing - original draft. **Qing Pei:** Validation. **Jian Wang:** Validation. **Zhanfeng Wang:** Resources. **Xiuli Hu:** Conceptualization, Resources, Supervision, Writing - review & editing, Data curation. **Zhigang Xie:** Resources, Supervision, Writing - review & editing.

Declaration of Competing Interest

The authors declare that they have no known competing financial interests or personal relationships that could have appeared to influence the work reported in this paper.

Acknowledgements

This work was financially supported by the National Natural Science Foundation of China (Project No. 51773197 and 51973214) and the Medical Health Industry Technology Project of Jilin Province (20180311070YY).

Appendix A. Supplementary data

Supplementary data to this article can be found online at https://doi.org/10.1016/j.jcis.2020.07.086.

References

[1] D. Peer, J.M. Karp, S. Hong, O.C. Farokhzad, R. Margalit, R. Langer, Nanocarriers as an emerging platform for cancer therapy, Nat. Nanotechnol. 2 (2007) 751–760.
[2] O. Taratula, B.S. Doddapaneni, C. Schumann, X. Li, S. Bracha, M. Milovancev, A. W.G. Alani, O. Taratula, Naphthalocyanine-based biodegradable polymeric nanoparticles for image-guided combinatorial phototherapy, Chem. Mater. 27 (2015) 6155–6165.
[3] C. Liang, L. Xu, G. Song, Z. Liu, Emerging nanomedicine approaches fighting tumor metastasis: animal models, metastasis-targeted drug delivery, phototherapy, and immunotherapy, Chem. Soc. Rev. 45 (2016) 6250–6269.
[4] D.C. Tormey, R. Gelman, P.R. Band, M. Sears, S.N. Rosenthal, W. Dewys, C. Perlia, M.A. Rice, Comparison of induction chemotherapies for metastatic breast cancer. An eastern cooperative oncology group trial, Cancer 50 (1982) 1235–1244.
[5] T. Nagy-Simon, M. Potara, A.M. Craciun, E. Licarete, S. Astilean, IR780-dye loaded gold nanoparticles as new near infrared activatable nanotheranostic agents for simultaneous photodynamic and photothermal therapy and intracellular tracking by surface enhanced resonant Raman scattering imaging, J. Colloid and Interface Sci. 517 (2018) 239–250.
[6] J. Lu, M. Liong, Z. Li, J.I. Zink, F. Tamanoi, Biocompatibility, biodistribution, and drug-delivery efficiency of mesoporous silica nanoparticles for cancer therapy in animals, Small 6 (2010) 1794–1805.
[7] J. Sudimack, R.J. Lee, Targeted drug delivery via the folate receptor, Adv. Drug Delivery Rev. 41 (2000) 147–162.
[8] A. Kumari, S.K. Yadav, S.C. Yadav, Biodegradable polymeric nanoparticles based drug delivery systems, Colloids Surf. B 75 (2010) 1–18.
[9] K. Cho, X. Wang, S. Nie, Z. Chen, D.M. Shin, Therapeutic nanoparticles for drug delivery in cancer, Clin. Cancer Res. 14 (2008) 1310.
[10] S.S. Suri, H. Fenniri, B. Singh, Nanotechnology-based drug delivery systems, J. Occup. Med. Toxicol. 2 (2007) 16.
[11] S.I. Stupp, L.C. Palmer, Supramolecular chemistry and self-assembly in organic materials design, Chem. Mater. 26 (2014) 507–518.
[12] Z. Luo, K. Cai, Y. Hu, L. Zhao, P. Liu, L. Duan, W. Yang, Mesoporous silica nanoparticles end-capped with collagen: redox-responsive nanoreservoirs for targeted drug delivery, Angew. Chem. Int. Ed. 50 (2011) 640–643.
[13] K. Kessenbrock, V. Plaks, Z. Werb, Matrix metalloproteinases: regulators of the tumor microenvironment, Cell 141 (2010) 52–67.
[14] T.L. Whiteside, The tumor microenvironment and its role in promoting tumor growth, Oncogene 27 (2008) 5904–5912.
[15] F. Danhier, O. Feron, V. Préat, To exploit the tumor microenvironment: Passive and active tumor targeting of nanocarriers for anti-cancer drug delivery, J. Controlled Release 148 (2010) 135–146.
[16] B. Fu, M. Dang, J. Tao, Y. Li, Y. Tang, Mesoporous platinum nanoparticle-based nanoplatforms for combined chemo-photothermal breast cancer therapy, J. Colloid Interface Sci. 570 (2020) 197–204.
[17] S.Z.F. Phua, C. Xue, W.Q. Lim, G. Yang, H. Chen, Y. Zhang, C.F. Wijaya, Z. Luo, Y. Zhao, Light-responsive prodrug-based supramolecular nanosystems for site-specific combination therapy of cancer, Chem. Mater. 31 (2019) 3349–3358.
[18] A. Laurent, C. Nicco, C. Chéreau, C. Goulvestre, J. Alexandre, A. Alves, E. Lévy, F. Goldwasser, Y. Panis, O. Soubrane, B. Weill, F. Batteux, Controlling tumor growth by modulating endogenous production of reactive oxygen species, Cancer Res. 65 (2005) 948.
[19] P.T. Schumacker, Reactive oxygen species in cancer cells: Live by the sword, die by the sword, Cancer Cell 10 (2006) 175–176.
[20] Y. Wang, J. Zhou, B. Zhang, L. Tian, Z. Ali, Q. Zhang, Fabrication and characterization of glutathione-imprinted polymers on fibrous SiO2 microspheres with high specific surface, Chem. Eng. J. 327 (2017) 932–940.
[21] M. Huo, J. Yuan, L. Tao, Y. Wei, Redox-responsive polymers for drug delivery: from molecular design to applications, Polym. Chem. 5 (2014) 1519–1528.
[22] C. Shi, X. Guo, Q. Qu, Z. Tang, Y. Wang, S. Zhou, Actively targeted delivery of anticancer drug to tumor cells by redox-responsive star-shaped micelles, Biomaterials 35 (2014) 8711–8722.
[23] C. Luo, J. Sun, D. Liu, B. Sun, L. Miao, S. Musetti, J. Li, X. Han, Y. Du, L. Li, L. Huang, Z. He, Self-assembled redox dual-responsive prodrug-nanosystem formed by single thioether-bridged paclitaxel-fatty acid conjugate for cancer chemotherapy, Nano Lett. 16 (2016) 5401–5408.
[24] B. Sun, C. Luo, X. Zhang, M. Guo, M. Sun, H. Yu, Q. Chen, W. Yang, M. Wang, S. Zuo, P. Chen, Q. Kan, H. Zhang, Y. Wang, Z. He, J. Sun, Probing the impact of sulfur/selenium/carbon linkages on prodrug nanoassemblies for cancer therapy, Nat. Commun. 10 (2019) 3211.
[25] L. Wang, F. Fan, W. Cao, H. Xu, Ultrasensitive ROS-responsive coassemblies of tellurium-containing molecules and phospholipids, ACS Appl. Mater. Interfaces 7 (2015) 16054–16060.
[26] C. Sun, L. Wang, B. Xianyu, T. Li, S. Gao, H. Xu, Selenoxide elimination manipulate the oxidative stress to improve the antitumor efficacy, Biomaterials 225 (2019) 119514.
[27] W. Zhang, W. Lin, Q. Pei, X. Hu, Z. Xie, X. Jing, Redox-hypersensitive organic nanoparticles for selective treatment of cancer cells, Chem. Mater. 28 (2016) 4440–4446.
[28] X. Zheng, L. Wang, S. Liu, W. Zhang, F. Liu, Z. Xie, Nanoparticles of chlorin dimer with enhanced absorbance for photoacoustic imaging and phototherapy, Adv. Funct. Mater. 28 (2018) 1706507.
[29] W. Zhang, W. Lin, X. Zheng, S. He, Z. Xie, Comparing effects of redox sensitivity of organic nanoparticles to photodynamic activity, Chem. Mater. 29 (2017) 1856–1863.
[30] J. Xia, T. Li, C. Lu, H. Xu, Selenium-containing polymers: perspectives toward diverse applications in both adaptive and biomedical materials, Macromolecules 51 (2018) 7435–7455.

[31] W. Cao, Y. Li, Y. Yi, S. Ji, L. Zeng, Z. Sun, H. Xu, Coordination-responsive selenium-containing polymer micelles for controlled drug release, Chem. Sci. 3 (2012) 3403–3408.
[32] T. Bai, D. Shao, J. Chen, Y. Li, B.B. Xu, J. Kong, pH-responsive dithiomaleimide-amphiphilic block copolymer for drug delivery and cellular imaging, J. Colloid and Interface Sci. 552 (2019) 439–447.
[33] X. Wang, X. Li, Y. Mao, D. Wang, Q. Zhao, S. Wang, Multi-stimuli responsive nanosystem modified by tumor-targeted carbon dots for chemophototherapy synergistic therapy, J. Colloid Interface Sci. 552 (2019) 639–650.
[34] L. Dai, R. Cai, M. Li, Z. Luo, Y. Yu, W. Chen, X. Shen, Y. Pei, X. Zhao, K. Cai, Dual-targeted cascade-responsive prodrug micelle system for tumor therapy in vivo, Chem. Mater. 29 (2017) 6976–6992.
[35] H. Xu, W. Cao, X. Zhang, Selenium-containing polymers: promising biomaterials for controlled release and enzyme mimics, Acc. Chem. Res. 46 (2013) 1647–1658.
[36] Z. Zhang, G. Chen, Y. Tang, Towards selenium recovery: Biocathode induced selenate reduction to extracellular elemental selenium nanoparticles, Chem. Eng. J. 351 (2018) 1095–1103.
[37] W. Cao, L. Wang, H. Xu, Selenium/tellurium containing polymer materials in nanobiotechnology, Nano Today 10 (2015) 717–736.
[38] L. Wang, W. Cao, H. Xu, Tellurium-containing polymers: towards biomaterials and optoelectronic materials, ChemNanoMat 2 (2016) 479–488.
[39] W. Zhang, R. Wang, W. Liu, X. Wang, P. Li, W. Zhang, H. Wang, B. Tang, Te-containing carbon dots for fluorescence imaging of superoxide anion in mice during acute strenuous exercise or emotional changes, Chem. Sci. 9 (2018) 721–727.
[40] Y. Wu, T. Guo, Y. Qiu, Y. Lin, Y. Yao, W. Lian, L. Lin, J. Song, H. Yang, An inorganic prodrug, tellurium nanowires with enhanced ROS generation and GSH depletion for selective cancer therapy, Chem. Sci. 10 (2019) 7068–7075.
[41] Q. Pei, X. Hu, L. Wang, S. Liu, X. Jing, Z. Xie, Cyclodextrin/paclitaxel dimer assembling vesicles: reversible morphology transition and cargo delivery, ACS Appl. Mater. Interfaces 9 (2017) 26740–26748.
[42] X. Han, J. Chen, M. Jiang, N. Zhang, K. Na, C. Luo, R. Zhang, M. Sun, G. Lin, R. Zhang, Y. Ma, D. Liu, Y. Wang, Paclitaxel-paclitaxel prodrug nanoassembly as a versatile nanoplatform for combinational cancer therapy, ACS Appl. Mater. Interfaces 8 (2016) 33506–33513.
[43] X. Wang, Y. Tian, X. Liao, Y. Tang, Q. Ni, J. Sun, Y. Zhao, J. Zhang, Z. Teng, G. Lu, Enhancing selective photosensitizer accumulation and oxygen supply for high-efficacy photodynamic therapy toward glioma by 5-aminolevulinic acid loaded nanoplatform, J. Colloid Interface Sci. 565 (2020) 483–493.
[44] R. Xia, X. Zheng, X. Hu, S. Liu, Z. Xie, Photothermal-controlled generation of alkyl radical from organic nanoparticles for tumor treatment, ACS Appl. Mater. Interfaces 11 (2019) 5782–5790.
[45] J.D. Bargh, A. Isidro-Llobet, J.S. Parker, D.R. Spring, Cleavable linkers in antibody–drug conjugates, Chem. Soc. Rev. 48 (2019) 4361–4374.
[46] H. Ye, Y. Zhou, X. Liu, Y. Chen, S. Duan, R. Zhu, Y. Liu, L. Yin, Recent advances on reactive oxygen species-responsive delivery and diagnosis system, Biomacromolecules 20 (2019) 2441–2463.
[47] Y. Cao, Y. Li, X.-Y. Hu, X. Zou, S. Xiong, C. Lin, L. Wang, Supramolecular nanoparticles constructed by DOX-Based prodrug with water-soluble pillar[6]arene for self-catalyzed rapid drug release, Chem. Mater. 27 (2015) 1110–1119.
[48] B. Sun, C. Luo, H. Yu, X. Zhang, Q. Chen, W. Yang, M. Wang, Q. Kan, H. Zhang, Y. Wang, Z. He, J. Sun, Disulfide bond-driven oxidation- and reduction-responsive prodrug nanoassemblies for cancer therapy, Nano Lett. 18 (2018) 3643–3650.
[49] Q. Pei, X. Hu, X. Zheng, R. Xia, S. Liu, Z. Xie, X. Jing, Albumin-bound paclitaxel dimeric prodrug nanoparticles with tumor redox heterogeneity-triggered drug release for synergistic photothermal/chemotherapy, Nano Res. 12 (2019) 877–887.
[50] D. Reichel, B. Sagong, J. Teh, Y. Zhang, S. Wagner, H. Wang, L.W.K. Chung, P. Butte, K.L. Black, J. Yu, J.M. Perez, Near infrared fluorescent nanoplatform for targeted intraoperative resection and chemotherapeutic treatment of glioblastoma, ACS Nano (2020).
[51] K.-H. Chen, Y.-B. Miao, C.-Y. Shang, T.-Y. Huang, Y.-T. Yu, C.-N. Yeh, H.-L. Song, C.-T. Chen, F.-L. Mi, K.-J. Lin, H.-W. Sung, A bubble bursting-mediated oral drug delivery system that enables concurrent delivery of lipophilic and hydrophilic chemotherapeutics for treating pancreatic tumors in rats, Biomaterials 255 (2020) 120157.
[52] G. Wang, D. Zhu, Z. Zhou, Y. Piao, J. Tang, Y. Shen, Glutathione-specific and intracellularly labile polymeric nanocarrier for efficient and safe cancer gene delivery, ACS Appl. Mater. Interfaces 12 (2020) 14825–14838.